Comprehensive study of the ^{6,7}Li $+\,^{124}$Sn reactions at energies near the Coulomb barrier

J. K. L. Chaves [1] L. R. Gasques [1,*] L. C. Chamon [1] V. Scarduelli [1] A. Lépine-Szily [1] W. A. Y. Hatano [1] and V. A. B. Zagatto[2]

[1]*Instituto de Fisica, Universidade de São Paulo, Rua do Matao 1371, 05508-090 São Paulo, São Paulo, Brazil*
[2]*Instituto de Física da Universidade Federal Fluminense, 24210-346 Niterói, Rio de Janeiro, Brazil*

Background: In recent decades, reactions involving weakly bound projectiles have been investigated by several research groups working in the nuclear physics field. Despite the relative success of a few theoretical models in addressing some reaction outcomes, many puzzling questions remain. A relatively large number of reactions with weakly bound nuclei have been systematically investigated at the Open Laboratory of Nuclear Physics of the University of São Paulo. The present data set is analyzed through coupled reaction channels calculations in the context of the double-folding São Paulo potential.

Purpose: The main goal of the present paper is to investigate nuclear reaction mechanisms for systems involving weakly bound projectiles.

Method: Angular distributions for several nuclear reaction processes were measured for the ^{6,7}Li $+\,^{124}$Sn systems at energies around the Coulomb barrier. Fusion data obtained in other works for both systems at energies below and above the barrier are also analyzed in the present paper.

Results: Angular distributions of elastic and inelastic scattering, as well as transfer, were obtained at the 30B scattering chamber of the Open Laboratory of Nuclear Physics of the University of São Paulo. The effect of the couplings to some nonelastic states on the angular distributions is discussed throughout the paper. Fusion cross sections were also analyzed using the coupled reaction channels approach. A strong absorptive imaginary potential is necessary to explain the measured angular distributions and fusion excitation functions.

Conclusion: The theoretical calculations within the coupled reaction channels formalism provide an overall good agreement with the corresponding elastic, inelastic, transfer, and fusion data.

I. INTRODUCTION

Owing to the binding energies with respect to the breakup into cluster structures, experiments involving weakly bound stable heavy-ion nuclei are of great importance to explore the properties of nuclei far from the valley of stability. In the last few decades, angular distributions and fusion data obtained for systems formed by weakly bound projectiles impinging on different targets have contributed to the development of theoretical models aiming to describe simultaneously different nuclear reaction outcomes [1–10].

In particular, ^{6,7}Li projectiles feature lowest separation energies as 1.47 and 2.47 MeV, respectively. They can be produced and accelerated in conventional particle accelerators, where the reactions with several targets allow systematic studies with high statistics. In previous experimental campaigns performed at the Open Laboratory of Nuclear Physics (LAFN, acronym in Portuguese), several reaction mechanisms such as elastic scattering, inelastic scattering and transfer around Coulomb barrier energies have been studied with the stable weakly bound projectiles ^{6}Li, ^{7}Li, and ^{10}B [6,7,11–16]. In the present paper, we report the measurement of angular distributions for the ^{6,7}Li $+\,^{124}$Sn reactions near Coulomb barrier energies. Besides the elastic channel, we have identified

yields corresponding to the inelastic excitation of the target for both systems, as well as the excitation of the ^{7}Li projectile for the ^{7}Li $+\,^{124}$Sn reaction. Moreover, one-neutron transfer events were experimentally observed for the ^{6}Li $+\,^{124}$Sn and ^{7}Li $+\,^{124}$Sn systems. The corresponding data were analyzed within the coupled reaction channel (CRC) formalism, where the nuclear interaction was described by the double-folding São Paulo potential (SPP) [17].

A simultaneous analysis of several reaction channels represents a challenge for theoretical models aiming to realistically describe their corresponding cross sections. Especially for reactions involving weakly bound projectiles, understanding the dynamics of the breakup process and its effect on the sub-barrier fusion still attracts strong interest in the nuclear physics community. Consequently, we have analyzed, using the same CRC approach, fusion excitation functions for the ^{6}Li $+\,^{124}$Sn and ^{7}Li $+\,^{124}$Sn reactions. The corresponding data were measured at energies below and above the barrier [18,19].

The paper is organized as follows. The experimental setup is presented in Sec. II. Results are discussed in Sec. III and a summary is given in Sec. IV.

II. EXPERIMENTAL DETAILS

The experiments were performed at the 30B scattering chamber of LAFN, São Paulo, Brazil. The incident ^{6,7}Li
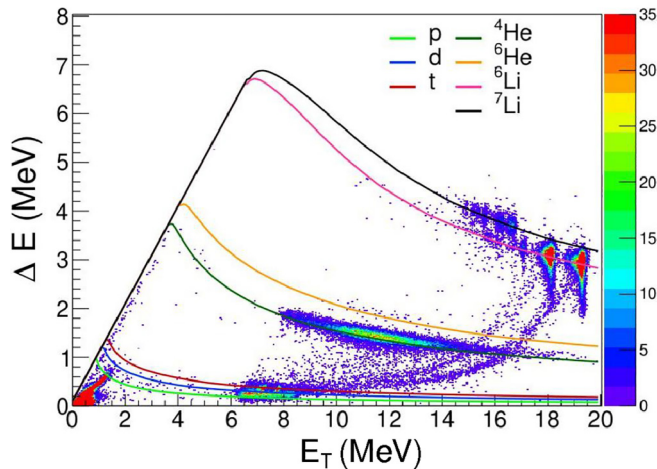
*Corresponding author: lgasques@if.usp.br

FIG. 1. ΔE-E_T spectrum obtained at $E_{Lab} = 21.5$ MeV and $\theta_{Lab} = 140°$ for the ^{6}Li + ^{124}Sn reaction. The lines correspond to theoretical calculations of energy loss in the ΔE detector for several identified nuclei produced during the collisions of projectiles on the target composed of ^{120}Sn and ^{197}Au.
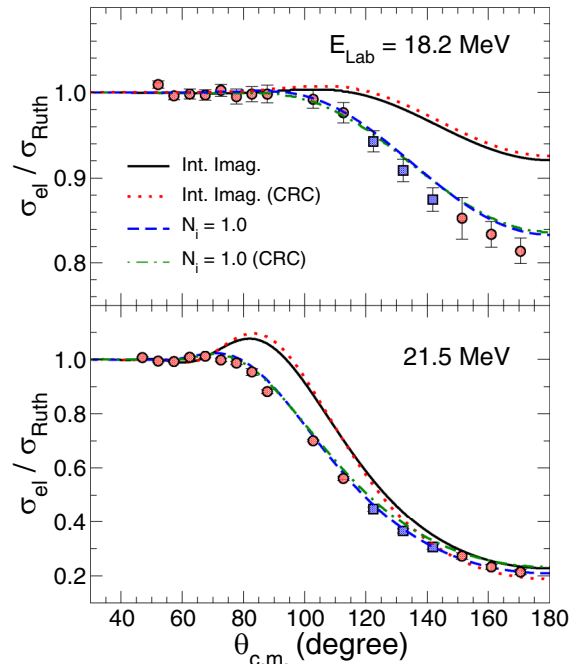

FIG. 2. Experimental cross sections for the elastic scattering of ^{6}Li + ^{124}Sn at two different bombarding energies. Theoretical results are represented by different lines (see text for details).

beams were produced by a multicathode source of negative ions by cesium sputtering (MC-SNICS) loaded with enriched lithium isotope cathodes and accelerated through an 8 MV tandem machine. Target foils of ^{124}Sn with thickness of around 70 μg/cm^2, evaporated onto about 5 μg/cm^2 carbon backing foils, were mounted at the center of the scattering chamber. For normalization purposes, a thin layer of ^{197}Au ($\approx$35 μg/cm^2) was evaporated over the ^{124}Sn films. Considering the thickness of the targets, the estimated energy loss of the lithium particles is about 15 KeV for all incident energies.

The SATURN (Silicon Array & Telescopes of USP for Nuclear Reactions and Nuclear Applications) array was used to detect the charged particles produced by the ^{6,7}Li + ^{124}Sn reactions. The array was composed of a set of semiconductor silicon surface barrier detectors (PIPs) mounted at approximately 30 cm from the target. Three PIPs were placed on a movable arm, covering forward angles in a range of $45° \leqslant \theta_{Lab} \leqslant 80°$, in steps of $5°$. At such forward angles, the elastic scattering cross sections are largely governed by the Coulomb interaction for the ^{6,7}Li + ^{124}Sn and ^{6,7}Li + ^{197}Au systems, which allows the normalization of the cross sections. Four other PIPs were mounted at $\theta_{Lab} = 100°$, $150°$, $160°$, and $170°$ on a fixed support. Three telescopes were also mounted on the same fixed support at $\theta_{Lab} = 120°$, $130°$, and $140°$. In this case, particle identification was possible based on the energy loss of different species crossing the ΔE first detection stage [20].

Figure 1 presents a typical two-dimensional (ΔE, E_T) spectrum obtained for ^{6}Li + ^{124}Sn at $E_{Lab} = 21.5$ MeV and $\theta_{Lab} = 140°$. E_T corresponds to the incident energy striking the telescope, while ΔE refers to the energy deposited in the first stage thin detector. Each band illustrated in the figure corresponds to the energy loss of different particles traversing the ΔE detector. The lines in the figure represent theoretical calculations for the energy loss in the ΔE detector as a function

of the total energy E_T of different nuclei. Elastic scattering yields of ^{6}Li on ^{124}Sn and ^{197}Au are clearly identified in the figure. They correspond to the two groups containing the highest counting rates. Events associated with the inelastic scattering of ^{6}Li + ^{124}Sn can also be observed in the same band. Due to the energy expended to populate an excited state of the projectile and/or target, they lie in the left side of the corresponding elastic scattering groups. The ^{7}Li events, arising from the one-neutron pickup transfer process, are also illustrated in the spectrum. Other groups, corresponding to $Z = 1$ and 2, are observed in Fig. 1. A possible explanation is that part of such yields are produced by the breakup of ^{6}Li (^{4}He − ^{2}H cluster). In addition, the observation of ^{4}He events can also be related to the fusion of ^{6}Li on carbon, which is present in the target, since the incident energy of the projectile is much higher than the Coulomb barrier for the ^{6}Li + ^{12}C reaction. A few counts lying in the ^{6}He band may have been produced by the direct single-charge exchange mechanism. Similar events have been observed in other measurements involving ^{6}Li and ^{10}B projectiles [7,15].

III. RESULTS AND DISCUSSION

Elastic scattering angular distributions were experimentally determined using the charged particle SATURN array. For both ^{6,7}Li + ^{124}Sn reactions, inelastic scattering cross sections associated with the first 2_1^+ (1.13 MeV) quadrupole state of the target were also determined in the experiment. In addition, yields corresponding to the one-neutron transfer channel were observed in the spectra for both reactions.
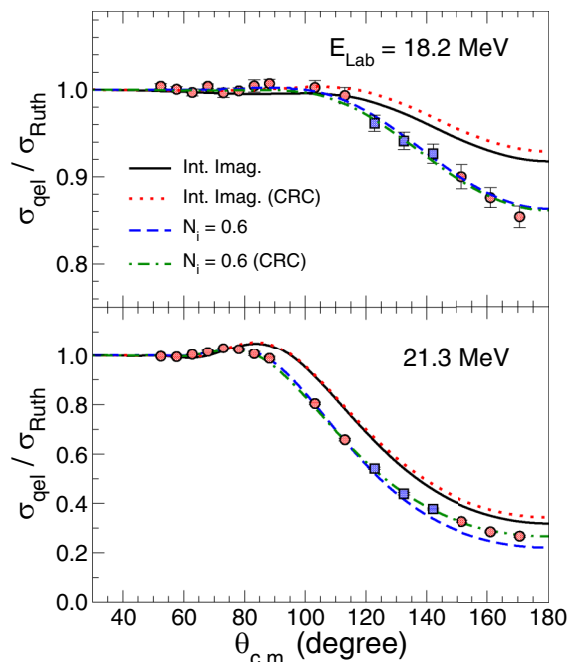
FIG. 3. Experimental cross sections for the quasielastic scattering of ^{7}Li + ^{124}Sn at two different bombarding energies. Theoretical results are represented by different lines (see text for details).

A. Elastic and inelastic angular distributions

Experimental elastic scattering angular distributions for the reactions ^{6}Li + ^{124}Sn and ^{7}Li + ^{124}Sn are presented in Figs. 2 and 3, respectively. The solid red circles and solid blue squares represent cross sections obtained with single detectors and telescopes, respectively. For each reaction, experimental data were obtained for two different bombarding energies, one
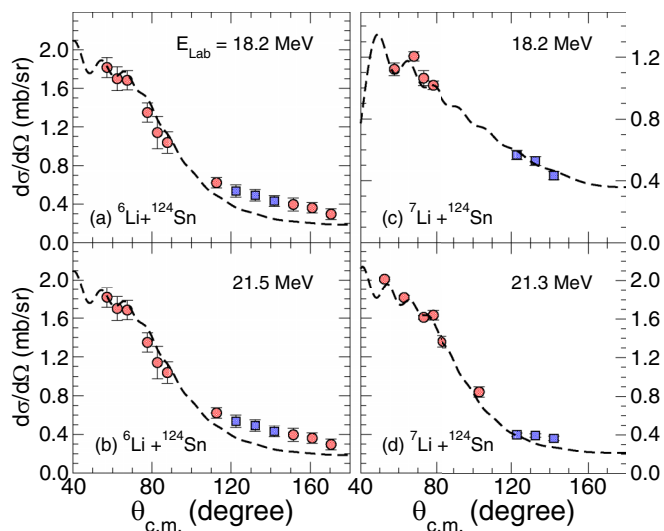

FIG. 4. Inelastic scattering angular distributions for the 2^+ quadrupole ^{124}Sn state at $E^* = 1.13$ MeV corresponding to the ^{6}Li + ^{124}Sn (a,b) and ^{7}Li + ^{124}Sn (c,d) reactions. The curves represent the theoretical results of the CRC calculations adopting $N_i = 1.0$ and 0.6 for the ^{6}Li + ^{124}Sn and ^{7}Li + ^{124}Sn, respectively (see text for details).

TABLE I. Spin, excitation energies (MeV), transition amplitudes from the ground state to the excited states (10^{-2} e^2b$^\lambda$), and deformation lengths (fm), for the inelastic states included in the CRC calculations.

Nucl.	Spin	E^*	λ	$B(E\lambda)\uparrow$	δ_λ	Ref.
^{6}Li	3^+	2.19	2	17.3	1.85	[23]
^{7}Li	$1/2^-$	0.477	2	7.59	2.77	[24]
^{124}Sn	2^+	1.13	2	16.3	0.55	[25]
^{124}Sn	3^-	2.60	3	9.89	0.62	[26]

below and one above the Coulomb barrier. Particularly, for the ^{7}Li + ^{124}Sn reaction, yields corresponding to the first $1/2^-$ excited state of the projectile ($E^* = 0.477$ MeV) are included in the elastic scattering cross sections data shown in Fig. 3. The same procedure was adopted in the calculations.

The data were compared with CRC calculations, which were carried out with the code FRESCO [21]. The SPP [17] was adopted to describe the real part of the optical potential. Table I presents $\lambda = 2$ and $\lambda = 3$ transition parameter values associated with the couplings of inelastic excitation channels of both projectile and target. The nuclear deformation, $\delta_\lambda = \beta_\lambda R$, was obtained from the Coulomb transition parameter, taking into account the correction due to the finite diffuseness value of the nuclear densities [22]. The curves exhibited in Figs. 2 and 3 are the results of theoretical calculations considering both single channel (no couplings) and CRC (inelastic and transfer couplings) approaches. The curves were obtained by (i) considering an internal imaginary potential (black solid and red dotted lines) or (ii) assuming an imaginary potential proportional to the SPP, $W(R) = N_i \times V_{SPP}$, where N_i was considered as an energy independent adjustable parameter (blue dashed and green dashed-dotted lines). Both assumptions result in quite different outputs. For the internal imaginary potential, we adopted a phenomenological Woods-Saxon (WS) parametrization with $W_0 = 50$ MeV, $r_{i0} = 0.8$ fm, and $a_i = 0.30$ fm. These parameters were set to account only for the absorption of flux following barrier penetration, resulting in negligible strength in the surface region. In order to accomplish a satisfactory description of the elastic scattering data, a strong absorptive imaginary potential is required. The best values of N_i are 1.0 and 0.6 for ^{6}Li + ^{124}Sn and ^{7}Li + ^{124}Sn, respectively. A comparison of all curves clearly shows that, although a relatively large N_i value is necessary to describe the data, the CRC approach provides only a small effect in the elastic channel. Similar results were obtained in Refs. [6,7]. These results might be explained by the predominant cluster structure and separation energy of the weakly bound ^{6,7}Li projectiles. Since they can split into two or more fragments with high probability in the field of the collision partner nucleus, the corresponding strong surface absorption could be related to breakup channel effects. Although couplings to continuum states might be important to investigate the effect of the breakup process in the elastic channel, such calculations are beyond the scope of the present work.

The experimental inelastic scattering angular distributions associated with the first 2^+ quadrupole ^{124}Sn state at
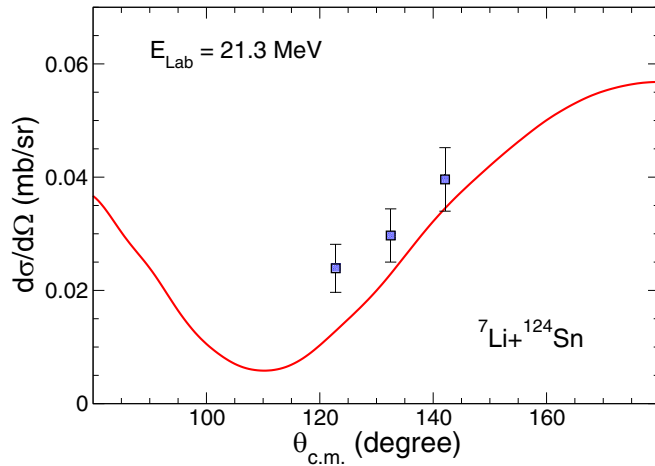
FIG. 5. Inelastic scattering angular distribution for the 3^- octopole ^{124}Sn state at $E^* = 2.60$ MeV corresponding to the ^{7}Li + ^{124}Sn reaction measured at $E_{Lab} = 21.3$ MeV. The red solid curve corresponds to the theoretical CRC calculations. The imaginary potential was obtained by adopting $N_i = 0.6$.

$E^* = 1.13$ MeV for both ^{6}Li + ^{124}Sn and ^{7}Li + ^{124}Sn reactions are represented in Fig. 4 by the solid red circles (single detectors) and solid blue squares (E-ΔE telescopes). The curves presented in the figure are the results of CRC calculations. As already mentioned, the theoretical cross sections were obtained by adopting $N_i = 1.0$ and 0.6 for ^{6}Li + ^{124}Sn and ^{7}Li + ^{124}Sn, respectively. The overall satisfactory agreement between data and theory is evident for all energies and systems. Nevertheless, at backward angles, where the collision dynamics is largely dominated by the nuclear interaction, the description of the ^{6}Li + ^{124}Sn data is somehow worse than that achieved for the ^{7}Li + ^{124}Sn reaction. The observation of such behavior might be related to the very low breakup threshold of the ^{6}Li projectile.

Figure 5 shows ^{7}Li + ^{124}Sn inelastic scattering angular distribution cross sections measured at $E_{Lab} = 21.3$ MeV. The solid blue squares refer to cross sections associated with the excitation of the 3^- octopole state ($E^* = 2.60$ MeV) of the ^{124}Sn target obtained with the three telescopes placed at $\theta_{Lab} = 120°$, $130°$, and $140°$. The CRC calculations shown by the solid red curve indicate that the data description is successful even though it is only provided in a limited angular range. Unfortunately, $\lambda = 3$ inelastic cross sections could not be experimentally resolved for the lowest bombarding energy, as well as for the ^{6}Li + ^{124}Sn reaction.

For completeness, we have also analyzed ^{7}Li + ^{124}Sn elastic and inelastic scattering angular distribution cross sections measured in an earlier work at $E_{Lab} = 28$ MeV [27]. The inelastic data, presented in Fig. 6, correspond to the excitation of the 1.13 MeV 2_1^+ [panel (b)] and 2.60 MeV 3_1^- [panel (c)] states of the target. As shown in Fig. 6 by the black solid curves, the shape and the order of magnitude of the elastic and inelastic angular distributions are well described by the theoretical results. Again, we have adopted $N_i = 0.6$ in the CRC calculations. Since no parameters were adjusted, and the description of the data measured at $E_{Lab} = 28$ MeV is quite reasonable, it is fair to conclude that the SPP interaction
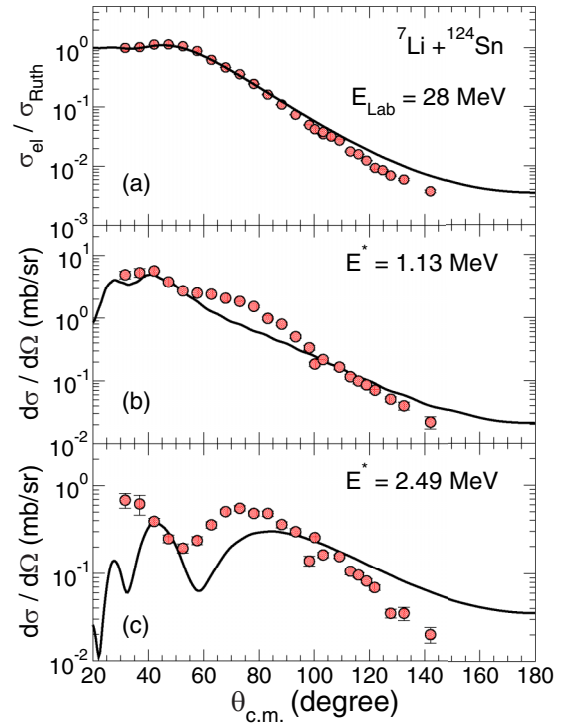

FIG. 6. Angular distribution cross sections for the ^{7}Li + ^{124}Sn reaction measured at $E_{Lab} = 28$ MeV [27]. Panel (a) shows the elastic scattering data, while panels (b) and (c) present the 2_1^+ and 3_1^- inelastic scattering angular distributions, respectively.
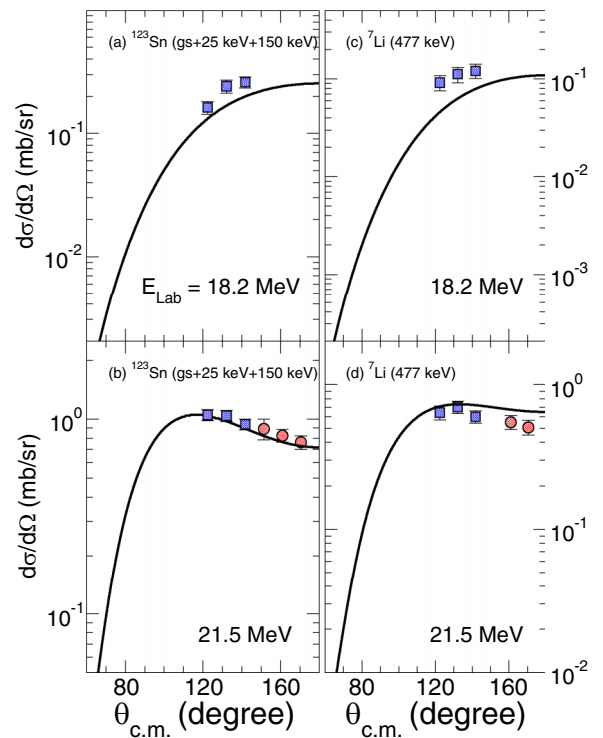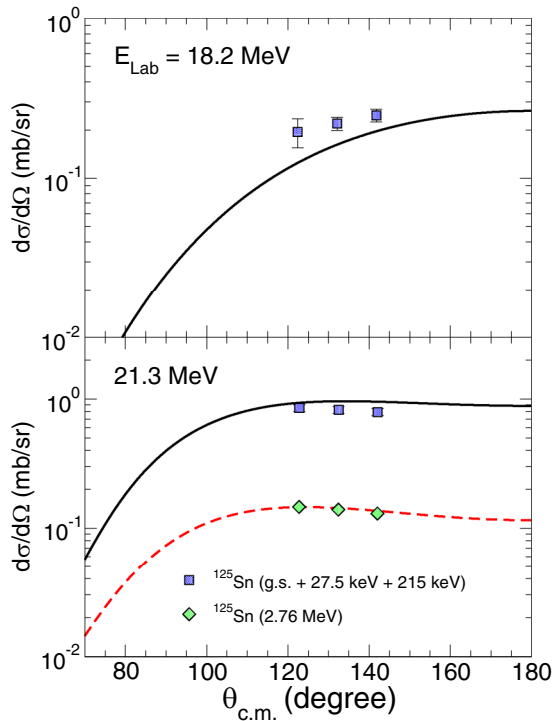

FIG. 7. Symbols represent the experimental cross sections for the one-neutron transfer process for the ^{6}Li + ^{124}Sn reaction. The curves are the results of CRC calculations (see text for details).

FIG. 8. Same as Fig. 7, for ^{7}Li + ^{124}Sn.

and the deformation lengths adopted in the CRC calculations are, in fact, realistic.

B. One-neutron transfer cross sections

Yields corresponding to the one-neutron pickup and stripping transfer channels were identified experimentally for the reactions ^{6}Li + ^{124}Sn and ^{7}Li + ^{124}Sn, respectively. The corresponding angular distributions cross sections were extracted and are plotted in Figs. 7 and 8.

The spectroscopic amplitudes (C^2S) used in the CRC calculations were mostly taken from the literature [28,29]. However, for some states, we have adjusted them to reproduce the data. The channels included in the CRC calculations, and their spectroscopic amplitudes, are listed in Table II. A WS shape was assumed for the particle-core potentials of the transfer reactions. We have adopted $R_0 = 2.4$ fm and 6.5 fm for Li+n and Sn+n, respectively. The diffuseness value was $a = 0.65$ fm for both cases. The depths V_0 of the WS potentials were adjusted by the code FRESCO to reproduce the experimental separation energies of the particle-core systems.

Concerning the ^{124}Sn(^{6}Li, ^{7}Li) ^{123}Sn reaction, the experimental angular distributions were obtained from the sum of yields related to the population of different states of the residual projectile and target nuclei. Panels (a) and (b) of Fig. 7 present experimental and theoretical CRC cross sections for one-neutron transfer relative to the ground-state (g.s.) and the first two excited states of the residual ^{123}Sn nucleus. The cross sections associated to the first ^{7}Li excited state (477 keV; $1/2^-$) are shown in panels (c) and (d) of Fig. 7. Data are shown for the two bombarding energies $E_{\text{Lab}} = 18.2$ and 21.5 MeV. For the lowest energy, yields could be experimen-

TABLE II. Energy levels of residual nuclei and spectroscopic amplitudes used for neutron transfer channels.

Nucleus	E^* (MeV)	J^π	C^2S	Ref.	C^2S (present work)
^{7}Li	0.000	$3/2^-$	0.90	[28]	
	0.477	$1/2^-$	1.15	[28]	2.72
^{123}Sn	0.000	$11/2^-$	4.49	[29]	
	0.025	$3/2^+$	4.49	[29]	2.00
	0.150	$1/2^+$	1.90	[29]	
	1.044	$7/2^+$	2.79	[29]	
	1.155	$7/2^+$	3.20	[29]	
	1.489	$5/2^+$	2.79	[29]	
^{125}Sn	0.000	$11/2^-$	0.42	[29]	
	0.027	$3/2^+$	0.44	[29]	
	0.215	$1/2^+$	0.33	[29]	
	1.260	$5/2^+$	0.07	[29]	
	2.760	$7/2^-$	0.54	[29]	1.10

tally observed only by the telescopes fixed at $\theta_{\text{Lab}} = 120°$, $130°$, and $140°$. As can be noticed in the figure, the agreement between data and CRC results can be considered satisfactory for both groups. However, it is important to mention that, as indicated in Table II, the spectroscopic amplitudes associated with the 477 keV excited state of the ^{7}Li and 25 keV excited state of the ^{123}Sn were adjusted to result in a better description of the data.

Figure 8 shows the one-neutron stripping angular distributions for the ^{7}Li + ^{124}Sn reaction measured at two bombarding energies: $E_{\text{Lab}} = 18.2$ and 21.3 MeV. The solid blue squares refer to the cross sections of the g.s. and the first two excited states of the residual ^{125}Sn nucleus, while the solid green diamonds are the transfer cross sections populating the ^{125}Sn excited state at 2.76 MeV. The black solid curves represent CRC results obtained as the sum of the contributions of each excited state of the ^{125}Sn nucleus. Although the theoretical results underestimate the data at the lowest bombarding energy and slightly overpredict the data at the highest bombarding energy, in general, the description of the corresponding data is satisfactory since any spectroscopic amplitude was adjusted in the calculations. On the other hand, to improve the description of the data associated to the 2.76 MeV excited state of the ^{125}Sn nucleus, its spectroscopic amplitude had to be adjusted (see Table II). Considering a value which is approximately twice the spectroscopic amplitude given in the literature [29], the CRC calculation, represented by the red dashed curve in Fig. 8, is in quite good agreement with the experimental data.

Most importantly, for both ^{6}Li + ^{124}Sn and ^{7}Li + ^{124}Sn reactions, the couplings to the one-neutron transfer channel do not significantly affect the theoretical cross sections for the elastic and inelastic processes. Similar results were obtained in previous works [6,7].

C. Fusion cross sections

For reactions involving weakly bound projectiles, complete fusion (CF) can present a suppression at above-barrier energies in comparison with the predictions of both the single
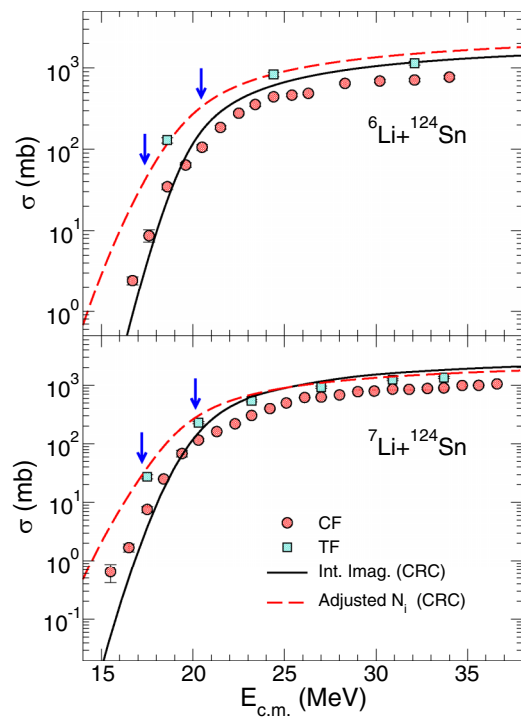
FIG. 9. Complete fusion (red solid circles) and total fusion (cyan solid squares) for the ^{6}Li + ^{124}Sn and ^{7}Li + ^{124}Sn reactions. The curves are the results obtained through CRC calculations adopting an internal imaginary WS potential (solid black lines) or assuming $N_i = 1.0$ and 0.6 for the ^{6}Li + ^{124}Sn and ^{7}Li + ^{124}Sn reactions, respectively. The blue arrows indicate the bombarding energies of the data taken in the present work.

barrier penetration (SBPM) and the CRC models [8,30–33]. Due to their low binding energy and cluster structure, weakly bound projectiles can break up prior to reaching the fusion barrier. In general, the missing CF cross sections are found in yields of incomplete fusion (ICF), which occurs when not all the fragments are captured by the target. The sum of CF and ICF, named total fusion (TF), is often predicted by SBPM and CRC approaches.

A simultaneous analysis of the cross sections of several different channels is quite important to proof test realistic models describing the dynamics of reaction mechanisms. Therefore, in the present paper, we have also studied fusion cross sections for the ^{6}Li + ^{124}Sn and ^{7}Li + ^{124}Sn reactions [18,19].

The results of the CRC calculations are compared with the experimental CF and TF cross sections in Fig. 9. The black solid curves were obtained assuming a phenomenological internal WS imaginary potential, with $W_0 = 50$ MeV, $r_{i0} = 0.8$ fm, and $a_i = 0.30$ fm. Adopting $N_i = 1.0$ and 0.6 for the ^{6}Li + ^{124}Sn and ^{7}Li + ^{124}Sn reactions, respectively, results in the red dashed curves. It is important to note that the theoretical results obtained by both SBPM and CRC models are quite similar in the entire energy range presented in Fig. 9. The effect of coupling inelastic and transfer states on the fusion cross sections is essentially negligible, and therefore the SBPM curves are not shown in the figure. Although it contradicts the results presented in Refs. [18,19], this observation is not

surprising. As indicated in Ref. [34], the effect of couplings on the fusion channel should become important to reactions with $\mu \gtrsim 8$, where μ is the reduced mass of the system. For ^{6}Li + ^{124}Sn and ^{7}Li + ^{124}Sn, $\mu = 5.7$ and 6.6, respectively. Nevertheless, at even lower bombarding energies, the effect of couplings on the fusion channel should become important. As a consequence, an enhancement on the cross sections is expected in comparison with the SBPM calculations.

As expected, the measured CF cross sections lie below the theoretical CRC calculations at energies above the barrier. On the other hand, the TF cross sections, measured at energies below and above the Coulomb barrier, are well described by the red dashed curves in Fig. 9, which were calculated by assuming $N_i = 1.0$ and 0.6 for ^{6}Li + ^{124}Sn and ^{7}Li + ^{124}Sn, respectively. The same assumption is required to describe the elastic, inelastic, and transfer cross sections through CRC calculations. This is a clear indication that, in the absence of explicitly taking the breakup channel into account, a strong absorption is required, not only in the inner barrier region but also in the surface, to predict the ^{6}Li + ^{124}Sn and ^{7}Li + ^{124}Sn cross sections.

IV. SUMMARY

Cross sections for elastic, inelastic, and one-neutron transfer reactions were measured for the ^{6}Li + ^{124}Sn and ^{7}Li + ^{124}Sn systems at two bombarding energies, one below and one above the Coulomb barrier. CRC calculations result in a general satisfactory description of the experimental angular distributions. For the bare interaction, the SPP was assumed. The adopted imaginary potential is proportional to the SPP, $W(R) = N_i \times V_{SPP}$, where N_i was considered as an energy independent adjustable parameter. The best values of N_i were 1.0 and 0.6 for ^{6}Li + ^{124}Sn and ^{7}Li + ^{124}Sn, respectively. For all bombarding energies, the effect of the couplings on the elastic channel is only marginal.

In our model, the imaginary potential simulates the absorption of flux from the elastic, inelastic, and transfer channels to the fusion process. By assuming an imaginary potential with strong absorption in the surface region, the TF cross sections are well described by the CRC calculations. As expected, for reactions involving weakly bound projectiles, the experimental CF cross sections lie below the theoretical CRC curves at energies above the fusion barrier.

We believe that systematic analyses of the available data using fully quantum-mechanical models that take into account more aspects of the three-body breakup channel, such as the continuum-discretized coupled-channel (CDCC) [35–37] or the Ichimura, Austern, and Vincent (IAV) [38] approach, might improve the description of the reaction mechanisms associated with collisions involving weakly bound projectiles.

[1] J. Szymakowski, K. W. Kemper, and A. D. Frawley, Nucl. Phys. A **355**, 221 (1981).

[2] M. Sinha, S. Roy, P. Basu, and H. Majumdar, Int. J. Mod. Phys. E **25**, 1650003 (2016).

[3] C. S. Palshetkar, S. Santra, A. Shrivastava, A. Chatterjee, S. K. Pandit, K. Ramachandran, V. V. Parkar, V. Nanal, V. Jha, B. J. Roy, and S. Kailas, Phys. Rev. C **89**, 064610 (2014).

[4] L. R. Gasques *et al.*, Phys. Rev. C **76**, 024612 (2007).

[5] J. C. Zamora *et al.*, Phys. Rev. C **84**, 034611 (2011).

[6] V. A. B. Zagatto, J. Lubian, L. R. Gasques, M. A. G. Alvarez, L. C. Chamon, J. R. B. Oliveira, J. A. Alcantara-Nunez, N. H. Medina, V. Scarduelli, A. Freitas, and I. Padron, E. S. Rossi, Jr., and J. M. B. Shorto, Phys. Rev. C **95**, 064614 (2017).

[7] V. A. B. Zagatto *et al.*, Phys. Rev. C **106**, 014622 (2022).

[8] M. Dasgupta *et al.*, Phys. Rev. C **70**, 024606 (2004).

[9] S. Kalkal, E. C. Simpson, D. H. Luong, K. J. Cook, M. Dasgupta, D. J. Hinde, I. P. Carter, D. Y. Jeung, G. Mohanto, C. S. Palshetkar, E. Prasad *et al.*, Phys. Rev. C **93**, 044605 (2016).

[10] J. J. Kolata, V. Guimarães, and E. F. Aguilera, Eur. Phys. J. A **52**, 123 (2016).

[11] L. R. Gasques *et al.*, Phys. Rev. C **97**, 034629 (2018).

[12] M. A. G. Alvarez *et al.*, Phys. Rev. C **98**, 024621 (2018).

[13] M. A. G. Alvarez *et al.*, Phys. Rev. C **100**, 064602 (2019).

[14] L. R. Gasques *et al.*, Phys. Rev. C **101**, 044604 (2020).

[15] L. R. Gasques *et al.*, Phys. Rev. C **103**, 034616 (2021).

[16] V. Scarduelli, L. R. Gasques, L. C. Chamon, V. A. B. Zagatto, M. A. G. Alvarez, and A. Lépine-Szily, Phys. Rev. C **106**, 044606 (2022).

[17] L. C. Chamon *et al.*, Phys. Rev. C **66**, 014610 (2002).

[18] V. V. Parkar *et al.*, Phys. Rev. C **98**, 014601 (2018).

[19] V. V. Parkar *et al.*, Phys. Rev. C **97**, 014607 (2018).

[20] V. Scarduelli, L. R. Gasques, L. C. Chamon, and A. Lépine-Szily, Eur. Phys. J. A **56**, 24 (2020).

[21] I. J. Thompson, Comput. Phys. Rep. **7**, 167 (1988).

[22] L. C. Chamon and B. V. Carlson, Nucl. Phys. A **846**, 1 (2010).

[23] A. T. Rudchik *et al.*, Phys. Rev. C **103**, 044614 (2021).

[24] W. J. Vermeer, R. H. Spear, and F. C. Barker, Nucl. Phys. A **500**, 212 (1989).

[25] B. Pritychenko, M. Birch, B. Singh, and M. Horoi, At. Data Nucl. Data Tables **107**, 1 (2016).

[26] P. J. van Hall, S. D. Wassenaar, S. S. Klein, G. J. Nijgh, J. H. Polane, and O. J. Poppema, J. Phys. G: Nucl. Part. Phys. **15**, 221 (1989).

[27] A. Kundu, S. Santra, A. Pal, D. Chattopadhyay, R. Tripathi, B. J. Roy, T. N. Nag, B. K. Nayak, A. Saxena, and S. Kailas, Phys. Rev. C **99**, 034609 (2019).

[28] J. P. Schiffer, G. C. Morrison, R. H. Siemssen, and B. Zeidman, Phys. Rev. **164**, 1274 (1967).

[29] V. V. Parkar, A. Parmar, Prasanna M., V. Jha, and S. Kailas, Phys. Rev. C **104**, 054603 (2021).

[30] M. Dasgupta, D. J. Hinde, R. D. Butt, R. M. Anjos, A. C. Berriman, N. Carlin, P. R. S. Gomes, C. R. Morton, J. O. Newton, A. Szanto de Toledo, and K. Hagino, Phys. Rev. Lett. **82**, 1395 (1999).

[31] P. R. S. Gomes *et al.*, Phys. Rev. C **73**, 064606 (2006).

[32] A. Mukherjee, R. Subinit, M. K. Pradhan, M. S. Sarkar, P. Basu, B. Dasmahapatra, T. Bhattacharya, S. Bhattacharya, S. K. Basu, A. Chatterjee, V. Tripathi, and S. Kailas, Phys. Lett. B **636**, 91 (2006).

[33] L. R. Gasques, D. J. Hinde, M. Dasgupta, A. Mukherjee, and R. G. Thomas, Phys. Rev. C **79**, 034605 (2009).

[34] L. R. Gasques, L. C. Chamon, D. Pereira, M. A. G. Alvarez, E. S. Rossi, Jr, C. P. Silva, and B. V. Carlson, Phys. Rev. C **69**, 034603 (2004).

[35] G. H. Rawitscher, Phys. Rev. C **9**, 2210 (1974).

[36] N. Austern, Y. Iseri, M. Kamimura, M. Kawai, G. Rawitscher, and M. Yahiro, Phys. Rep. **154**, 125 (1987).

[37] P. Descouvemont, L. F. Canto, and M. S. Hussein, Phys. Rev. C **95**, 014604 (2017).

[38] J. Lei and A. M. Moro, Phys. Rev. C **92**, 044616 (2015).